

Phase-Resolving Wave Propagation Array Models

P. Troch, V. Stratigaki

Department of Civil Engineering, Ghent University, Ghent, Belgium

10.1 INTRODUCTION

This chapter describes the use of a phase-resolving wave propagation model for assessing the park effect in arrays of wave energy converters (WECs) and the far-field wake effects of the arrays. The applied wave propagation model, MILD-wave, is based on the mild-slope equations (see, eg, [Radder and Dingemans, 1985](#)), simulating the propagation and transformation of water waves in time over relatively large distances, and is used for all the examples provided in this chapter. However, the generic numerical techniques presented here are also applicable to models based on the Boussinesq equations (see, eg, [Madsen and Sørensen, 1992](#)). The use of these equations adds nonlinearity to the waves in shallow water conditions, but at a higher computational cost and with more numerical instability issues.

The implementation of the WEC (array) is carried out using the numerical techniques of so-called sponge layers and wave generation along a circle, to simulate the physical process of energy absorption by the WEC, and the resulting wave transformation processes of reflection, diffraction, and radiation. The motivation for

using (time marching) phase-resolving wave propagation models for modelling the effects and interactions in WEC array lies in

- the potential to model (very) large domains at a reasonable computational cost, in the order of tens of kilometres;
- the ability to model the impact of the WEC array at larger distances, and thus the effects on the coastline or other stakeholders at sea;
- the potential to use a nested (or coupled) approach for modelling both near-field (park) effects and far-field (wake) effects;
- the intrinsic inclusion of diffraction in the mild-slope equations (compared to phase-averaging models where a parameterized approach is applied).

A good knowledge of the physical processes of wave interaction with a WEC is required for a full understanding of WEC farm effects and their implementation. When the WEC interacts with the incident wave field and absorbs wave energy from the incident wave field, additional wave fields are generated. These are the reflected, diffracted, and radiated wave fields. Incident waves are usually assumed as plane waves propagating

in one direction. Reflected, diffracted, and radiated waves propagate in every direction from the WEC source location as circular waves. As a result, some energy from the incident waves is redistributed from a single direction into all other directions, thereby affecting the other WECs around the WEC.

Assuming linear wave theory, all wave fields can be easily superimposed by applying the superposition principle, and all are described by the same linear wave theory. The reflected and diffracted wave fields are usually associated with the presence of a fixed WEC in the incident wave field, whereas the radiated wave field is generated by the motion response (realizing the energy absorption) of the WEC in the incident wave field. The total wave field, also called the perturbed wave field, is the superposition of all mentioned wave fields: incident waves + reflected waves + diffracted waves + radiated waves.

Fig. 10.1 shows a typical example of a numerically calculated wave interaction with a 3×3 farm of overtopping WECs. The contour plot shows the values of the wave heights in plan view (as a disturbance coefficient K_d), resulting from the absorption of wave energy out of the incident long-crested wave field (incident waves propagate from bottom to top). In front of the farm, a uniform undisturbed wave field is present. Inside the farm, there is interaction between the individual WECs and the scattered wave fields they generate, resulting in a somewhat different response of each WEC to the incident waves: this is the so-called park effect (or intra-array effect) in an array of WECs. Behind the farm, on the leeside, a wake of reduced wave heights is seen, extending over a larger distance behind the farm: this is the so-called far-field effect (or extra-array effect).

We apply a classification into two generic types of WECs, for the implementation of WECs

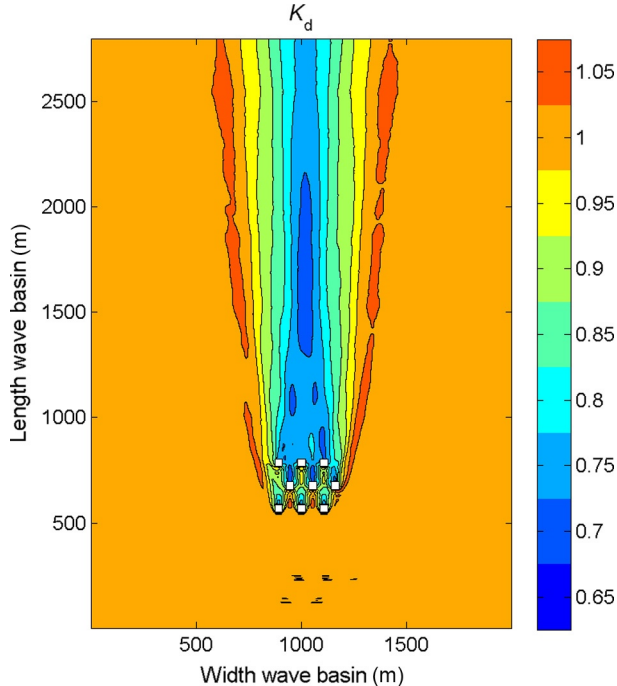


FIG. 10.1 A typical example of wave interaction with a farm of 3×3 WECs, and the resulting wake, visualized using the disturbance coefficient K_d , for irregular long-crested head-on waves with $T_p = 5.2$ s.

in the wave propagation model, based on the significance of the radiated wave field. Firstly, when WECs do not move under incident waves (type (a) WECs), the radiated waves are negligible. An example of this type of WEC is the WEC of the overtopping type (such as the Wave Dragon). Secondly, when WECs move under incident waves (type (b) WECs), such as is the case for, eg, point-absorbers, the radiated wave field is significant and needs explicit treatment.

A type (a) WEC is implemented in the phase-resolving wave propagation model as an array of cells (geometrically covering the spatial extent of the WEC) which has been assigned a given degree of reflection, absorption, and transmission using the sponge layer technique. Absorption functions define the absorption coefficient S attached to each cell of the WEC. By changing the values of the absorption coefficients or the number of absorbing cells, the degree of reflection and transmission and therefore absorption (based on conservation of energy) of the WEC structure can be modified, and tuned towards the target values of reflection and transmission characteristics of the WEC.

In general, sponge layers are typically used at the boundaries of the numerical domain to avoid unwanted reflection from the boundaries, targeting a very small amount of reflection. In the case of WECs, the degree of reflection will be larger, and transmission also becomes important. Sponge layers have sometimes other names (such as porosity blocks or layers, sinks, partial transmitting, and reflecting obstacles, etc.) and slightly varying implementations (eg, the explicit treatment in the equations by an extra absorption term), but represent basically the same idea of dissipating artificially part of the energy in the incident waves.

Where wave radiation becomes significant, ie, for type (b) WECs, the sponge layer technique is extended with additional wave generation along a circle around the WEC, to simulate the generation of the radiated wave field. The characteristics of the radiated wave field (surface elevations

and phase angles) are adopted from a wave-WEC model (or wave-structure solver) which simulates the hydrodynamics in detail, along the same circle around the WEC, and are subsequently used as input on the wave generation circle. This way, an efficient coupling between the wave propagation model and the wave-WEC interaction model, such as a boundary element method (BEM) model, is realized.

The coupling can also be regarded as nesting of a model, representing the detailed prediction of the WEC interaction with the waves, into the wave propagation model. The degree of detail in the prediction can be chosen by selecting the appropriate model: either using the semi-empirically calibrated sponge layer technique (Beels et al., 2010a), or using the analytically obtained Kochin functions for the far-field description of the velocity potential (Babarit et al., 2013), or using the numerically predicted wave field obtained from a potential-flow solver or a Navier-Stokes solver (McNatt et al., 2013; Mei et al., 2005). This versatile coupling avoids the limitations in computational cost of wave-WEC models and allows the modelling of environmental impacts of WEC farms.

In the rest of this chapter, the implementation of a WEC and a WEC farm in MILDwave is described. After a short presentation of the theoretical background of MILDwave and the solution algorithm, wave generation is discussed, with special attention to wave generation on a circle. Subsequently, the implementation of the sponge layer technique is presented in detail for a single type (a) WEC and reference is made for the case of a farm of type (a) WECs. A general introduction into the new coupling methodology for both a single WEC and a WEC farm is given at the end of Section 10.2. In Section 10.3, this approach is applied in a practical situation, to study the wave height reduction behind a single and a farm of type (a) WECs, and a single type (b) WEC. Finally, in Section 10.4, the limitations of the array model are discussed and the chapter is summarized in Section 10.5.

10.2 IMPLEMENTATION OF THE WEC SIMULATION IN THE WAVE PROPAGATION MODEL MILDWAVE

10.2.1 General Formulation of MILDwave

The phase-resolving model MILDwave ([Stratigaki and Troch, 2012a](#)) is a mild-slope wave propagation model, initially developed by [Troch \(1998\)](#). MILDwave is able to generate linear water waves over a mildly varying bathymetry. Bathymetries (with mild slopes) can be modelled accurately, since the model has mostly been applied for fine grid cell sizes. The model calculates instantaneous surface elevations throughout the domain, with a relatively low computational and accuracy cost and with high stability. Wave transformation processes such as refraction, shoaling, reflection, transmission, and diffraction are simulated intrinsically, and the processes of wave breaking and wave growth by wind are simulated using parameterized models. MILDwave can generate regular and irregular long- and short-crested waves, along lines, and circles. A typical application of the model is the study of wave penetration in harbours, eg, Zeebrugge and Ostend in Belgium (eg, [Stratigaki and Troch, 2010a; Stratigaki et al., 2010, 2011; Gruwez et al., 2012a,b](#)) and Hanstholm in Denmark ([Margheritini et al., 2010, 2011, 2012; Stratigaki et al., 2012b](#)). Several wave transformation studies have been carried out using MILDwave, eg, along the Norwegian coast ([Kofoed et al., 2008](#)) and along the Belgian coast for the Thorntonbank, Flanders Bays ([Stratigaki and Troch, 2010b, 2012b; Stratigaki et al., 2012a](#), etc.).

Based on the initial derivation of the elliptic mild-slope wave equation by [Berkhoff \(1972\)](#), the parabolic model ([Radder, 1979](#)) and the hyperbolic model ([Copeland, 1985](#)) have been developed to study the propagation of monochromatic waves in larger coastal areas. In the parabolic model wave reflection and diffraction in the direction of wave propagation are neglected.

Time-dependent mild-slope equations have been developed to study the transformation of random waves with a narrow frequency band. [Radder and Dingemans \(1985\)](#) have derived a canonical form of the time-dependent mild-slope equations based on the Hamiltonian theory of surface waves, taking into account the mild-slope assumption $|\nabla h|/kh \ll 1$, where ∇ is the horizontal gradient operator, h the water depth and k the wave number. [Booij \(1983\)](#) proved that the equations were only valid for a bed steepness up to 1/3. [Suh et al. \(1997\)](#) extended the latter model to study wave propagation on a rapidly varying impermeable bathymetry by considering higher-order bottom-effect terms proportional to the square of bottom slope and to the bottom curvature. A detailed review of the evolution of the mild-slope equations can be found in [Dingemans \(1997\)](#). The mild-slope equations of [Radder and Dingemans \(1985\)](#) without the extension of [Suh et al. \(1997\)](#) are the basic equations in the phase-resolving model MILDwave, presented here.

MILDwave makes use of the hyperbolic depth-integrated mild-slope equations of [Radder and Dingemans \(1985\)](#). For regular waves, these equations are expressed by (Eq. 10.1)

$$\left\{ \begin{array}{l} \frac{\partial \eta}{\partial t} = \frac{\omega^2 - k^2 C C_g}{g} \phi - \nabla \cdot \left(\frac{C C_g}{g} \nabla \phi \right) \\ \frac{\partial \phi}{\partial t} = -g\eta \end{array} \right. \quad (10.1)$$

where η and ϕ are, respectively, the surface elevation and the velocity potential at the free water surface, ∇ is the horizontal gradient operator, t is the time, g is the gravitational acceleration, C is the phase velocity and C_g the group velocity for a wave with wave number k and angular frequency ω .

A detailed derivation of these equations can be found in [Radder and Dingemans \(1985\)](#). For irregular waves, C , C_g , k_w and ω are replaced in (Eq. 10.1) by the wave characteristics for the carrier frequency \bar{f} , ie, \bar{C} , \bar{C}_g , \bar{k}_w and $\bar{\omega}$. In [Stratigaki et al. \(2011\)](#), the equations are

extended in order to account in MILDwave for depth-induced wave breaking and wave growth by wind, and the wave propagation model is solved using a finite difference scheme that consists of a two-step space-centred, time-staggered computational grid, as described in Brorsen and Helm-Petersen (1998). In MILDwave waves are generated at the offshore boundary by using the source term addition method, ie, by adding an additional surface elevation η^* to the calculated value on a wave generation line for each time step (Lee and Suh, 1998). Furthermore, Lee and Suh (1998) have proven that the model of Radder and Dingemans (1985) can be used to simulate the transformation of long- and short-crested random waves.

10.2.2 Wave Generation on a Circle (for Radiated Waves)

WECs (like point-absorbers) which absorb part of the incident wave energy respond by featuring a heave motion which, in turn, generates a radiated wave field. In MILDwave, radiated wave fields are implemented by wave generation on a circle, based on the study by Lee and Suh (1998). The technique implemented in MILDwave was developed by Troch and Beels (2009) and recently has been adopted by Babarit et al. (2013) for modelling WECs in another wave propagation model. The method essentially uses the principle of conservation of energy to determine the waves that need to be generated on a wave generation circle. However in MILDwave, it is observed that this leads to an inaccuracy in the wave amplitude and so therefore an iterative approach is used.

10.2.3 Implementation of the Sponge Layer Technique

A number of examples exist in the literature of the use of a sponge layer to represent a WEC or WEC farm. In Mendes et al. (2008) the wave height (for regular waves only) and wave

direction on the 10 m water depth contour behind two configurations of farms of Pelamis WECs, both with a total installed capacity of 202.5 MW and a total length of 16 km, have been assessed in the mild-slope model REF/DIF. Each farm was modelled as an energy dissipating area in the computational domain. For both configurations the maximum observed wave height change was less than 15%. In Vidal et al. (2007) an overall wave height transmission coefficient of a farm of PowerBuoys was calculated (=0.96) to study the coastal impact in a mild-slope wave propagation model. A negligible coastal impact of the farm was observed. In Venugopal and Smith (2007) five bottom mounted, fixed WECs were implemented as individual porous structures with a prescribed degree of porosity in a nonlinear Boussinesq wave model (MIKE 21 BW).

These implementations of the sponge layer technique have a number of limitations. Firstly, the models of Mendes et al. (2008) and Vidal et al. (2007) simplify a farm to one transmitting obstacle. Thus, the redistribution of wave energy around the WECs in the farm due to (i) an alternation of full (gaps between the WECs) and partial transmission (through the WECs), (ii) diffraction, and (iii) radiation (floating WECs), is not taken into account. Secondly, in the study of Venugopal and Smith (2007), the obtained value of transmission cannot be changed after setting the value of reflection through the degree of porosity of the structure (by using a constant value for all cells of the WEC), which makes the adaptation to the incident wave climate of a WEC inside a farm impossible.

These limitations can be avoided by modelling each WEC individually and modifying the shape of the absorption function throughout the WEC, as has been first presented by Troch et al. (2010) and Beels et al. (2010a,b,c). This way, the degree of absorption (and consequently transmission) of the WEC, prescribed in the power matrix of the WEC, can be tuned for a fixed amount of reflection on the WEC, as specified by the developer.

In this section this technique is described to simulate WECs of type (a), using an example of a WEC based on the overtopping principle. Incident waves are partly reflected on the WEC, partly overtopped in the basin and consequently absorbed and partly transmitted under and around the structure. The degree of absorption, as a function of the incident wave climate, can be derived based on a power matrix from the WEC developer; the amount of reflection on the structure can also be specified by the developer. When the amounts of absorption and reflection are known, the WEC can be modelled.

In MILDwave the WEC is represented by an array of cells (covering the spatial extensions of the WEC) that have been assigned a given degree of absorption using the sponge layer technique. Absorption functions $S(x)$ or $S(y)$ define the absorption coefficient S attached to each cell of the WEC in x -direction and y -direction, respectively. By changing the values of the absorption coefficients or the number of absorbing cells, the degree of reflection and transmission and consequently absorption of the porous structure can be modified. If a constant absorption coefficient S is used for all cells of the WEC, the amount of reflection, transmission, and absorption are coupled as seen in [Venugopal and Smith \(2007\)](#). In other words, for a specific realized value of the reflection coefficient, only one (fixed) value for the transmission coefficient can be obtained, thereby not allowing to tune the transmission value to the target value. To avoid

this coupled dependency, different absorption functions can be used to tune the degree of absorption (and consequently transmission) for a fixed amount of reflection on the WEC.

To define the reflection, transmission and consequently absorption characteristics of a WEC a structure composed of a series of absorbing cells is implemented in a numerical test flume ([Fig. 10.2](#)). This simplified model is used to determine the absorption function $S(x)$ and $S(y)$ required to obtain the desired reflection, transmission, and absorption characteristics.

Two parameters can be varied to tune the WEC for a given sea-state: the value of the absorption coefficients ([Section 10.2.3.1](#)) and the absorption length ([Section 10.2.3.2](#)). Using the proposed methodology, it is possible to achieve a frequency dependent absorption, as will be shown in [Section 10.2.3.3](#).

10.2.3.1 Influence of the Absorption Coefficient on the Absorption Characteristics

As an example of the influence of the absorption function, a WEC with a length of 36 m and with a constant absorption coefficient $S(x)=S(y)=S$ along its length has been implemented in the wave flume ([Fig. 10.3A](#)). The reflection coefficient K_r and the transmission coefficient K_t are shown in [Fig. 10.4](#) for values of S between 0.8 and 1 as a function of the value used for S .

[Fig. 10.5](#) gives the degree of power absorption, which equals the proportion of incident power not transmitted or reflected ($1-K_t^2-K_r^2$),

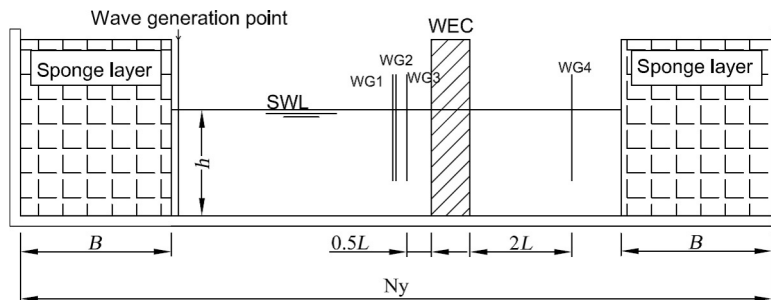


FIG. 10.2 Definition sketch of numerical test flume—cross section.

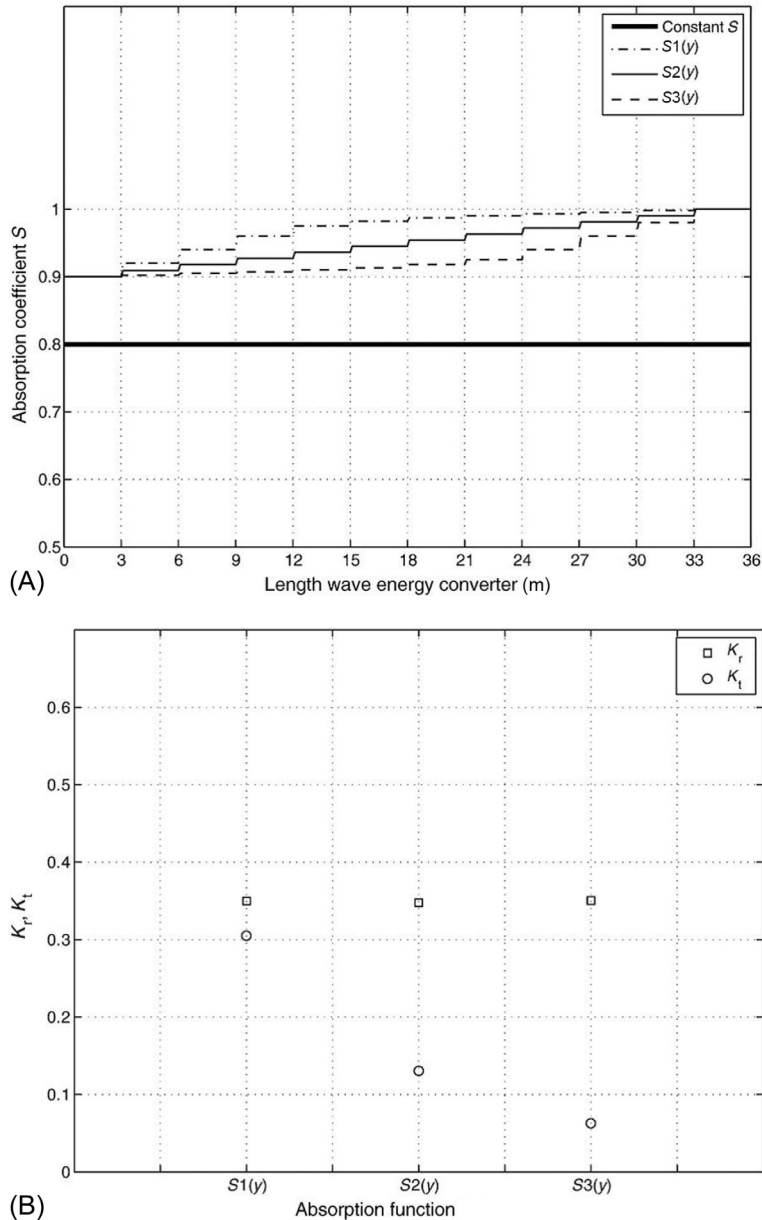


FIG. 10.3 (A) Change in absorption coefficient S through the WEC. (B) Reflection coefficient K_r and transmission coefficient K_t for three different shapes of the absorption function $S(y)$.

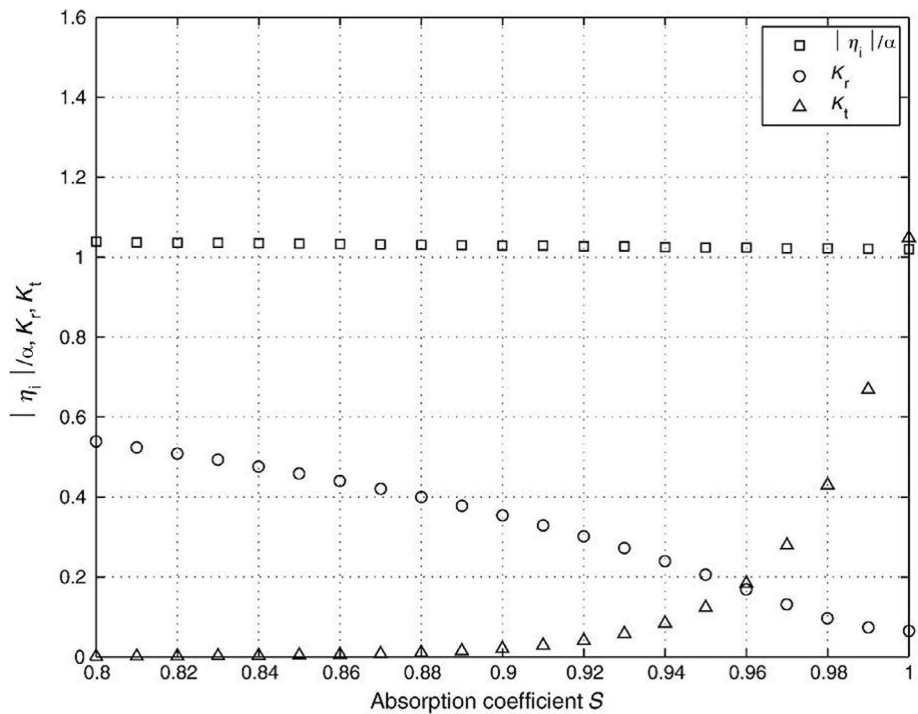


FIG. 10.4 Dimensionless measured wave amplitude $\frac{|\eta_i|}{\alpha}$, reflection coefficient K_r and transmission coefficient K_t for a WEC of 36 m with a constant absorption coefficient S , ranging from 0.8 to 1.0 (regular waves, $T=5.2$ s, $H=1.0$ m, $H=30$ m).

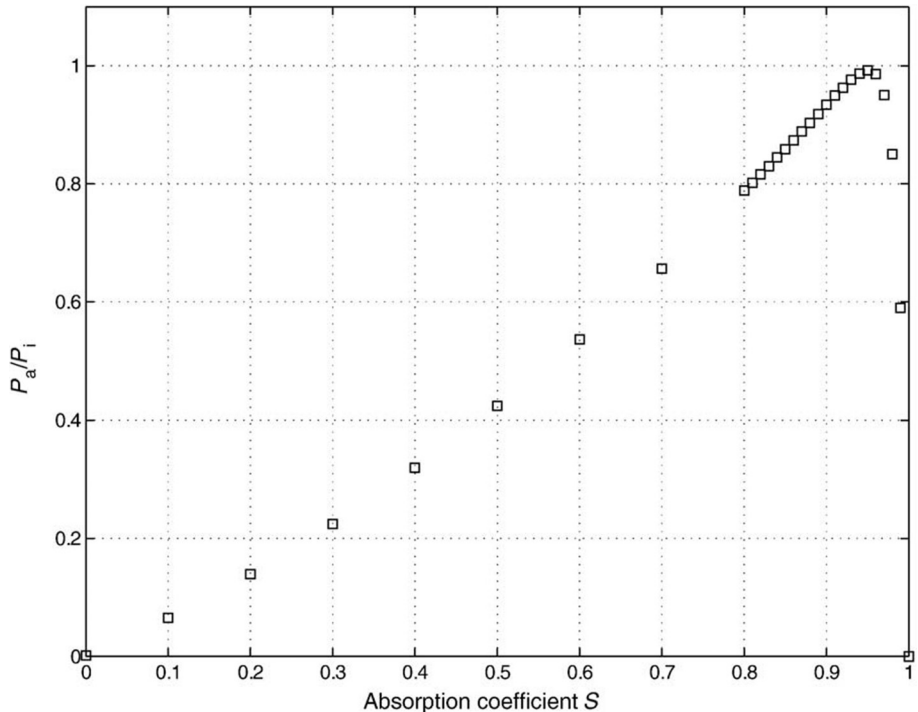


FIG. 10.5 Dimensionless absorbed wave power, P_a/P_i , for a WEC of 36 m with a constant absorption coefficient S , ranging from 0 to 1 (regular waves, $T=5.2$ s, $H=1.0$ m, $H=30$ m).

as a function of the absorption coefficient S . As Fig. 10.5 shows, any level of absorption can be modelled, but each level of absorption is paired with a specific amount of reflection and transmission (as seen on Fig. 10.4). Thus, it is not possible to define the absorption, reflection, and transmission coefficients independently using a constant absorption coefficient: for example, if we consider a WEC of 36 m length with a reflection coefficient of 0.1 which is absorbing 80% of the incident wave power. To obtain a reflection coefficient of 0.1, the WEC should consist of cells with an absorption coefficient of 0.98 (Fig. 10.4); however, an absorption coefficient of 0.8 (Fig. 10.5) is needed to obtain the required amount of absorbed power.

The decoupling of reflection and absorption can be achieved by changing the shape of the absorption function S through the WEC. As an example, a WEC with a reflection coefficient of 0.35 (which means that 12% of the incident wave power is reflected) and three different curves of the absorption coefficient through the WEC, $S_1(y)$, $S_2(y)$, and $S_3(y)$ are modelled as shown in Fig. 10.3A. These produce a range of degrees of absorption of 78%, 86%, and 87%, respectively.

The effect of the three different curves on the value of the reflection coefficient K_r is minimal (Fig. 10.3B) as the degree of reflection is only influenced by the value of S for the edge cells of the WEC (Beels et al., 2010a). The value of K_r in Fig. 10.3B for $S_3(y)$ (where the modelled degree of absorption is 87%) remains almost equal to the value of K_r for a constant absorption coefficient $S=0.9$ as shown in Fig. 10.4. On the other hand the degree of transmission is clearly affected by the variation of S through the WEC (Fig. 10.3B). When using $S_2(y)$ and $S_3(y)$ almost no wave power is transmitted. On the other hand when $S_1(y)$ is implemented, K_t is approximately 15 times higher than K_t for $S=0.9$ in Fig. 10.4.

By changing the shape of the absorption function $S(y)$ through the structure, the amount of transmission and consequently absorption is

made independent of the amount of reflection. This way the degree of absorption (and consequently transmission) of the WEC, derived from the power matrix of the WEC, can be tuned for a fixed amount of reflection on the WEC.

10.2.3.2 Influence of Length on the Absorption Characteristics

For large absorption coefficients a longer obstacle is required to achieve the amount of absorption. It is found that the maximum amount of absorbed wave power of the implemented WEC depends on the dimensions (ie, length) of the WEC. Specifically, when modelling a WEC smaller than approximately 18 m an absorption of 100% cannot be obtained, even by decoupling the reflection and transmission, as the number of cells required to vary the absorption coefficient is too small. However, this is not considered to be a significant limitation since a small WEC is unlikely to have a 100% absorption characteristic and WECs based on the overtopping principle typically have sufficiently large dimensions to model the required level of absorption.

10.2.3.3 Frequency Dependent Absorption

For a real WEC the power absorption varies with frequency. However, the frequency also influences the relationship between the reflection and transmission coefficients for a given absorption function S . The reflection and transmission coefficients for different WEC lengths and wave periods using a constant absorption coefficient $S=0.9$ are presented in Fig. 10.6A and B. It can be seen that the amounts of reflection and transmission increase with the wave period, with the increase in K_t greater than the increase of K_r . Consequently, the absorbed wave power decreases with increasing wave period as the amounts of reflection and transmission increase with increasing wave period (Fig. 10.6B). It has also been shown that the significance of the wave period is greater for larger value of S (Beels et al., 2010a). Consequently, the reflection

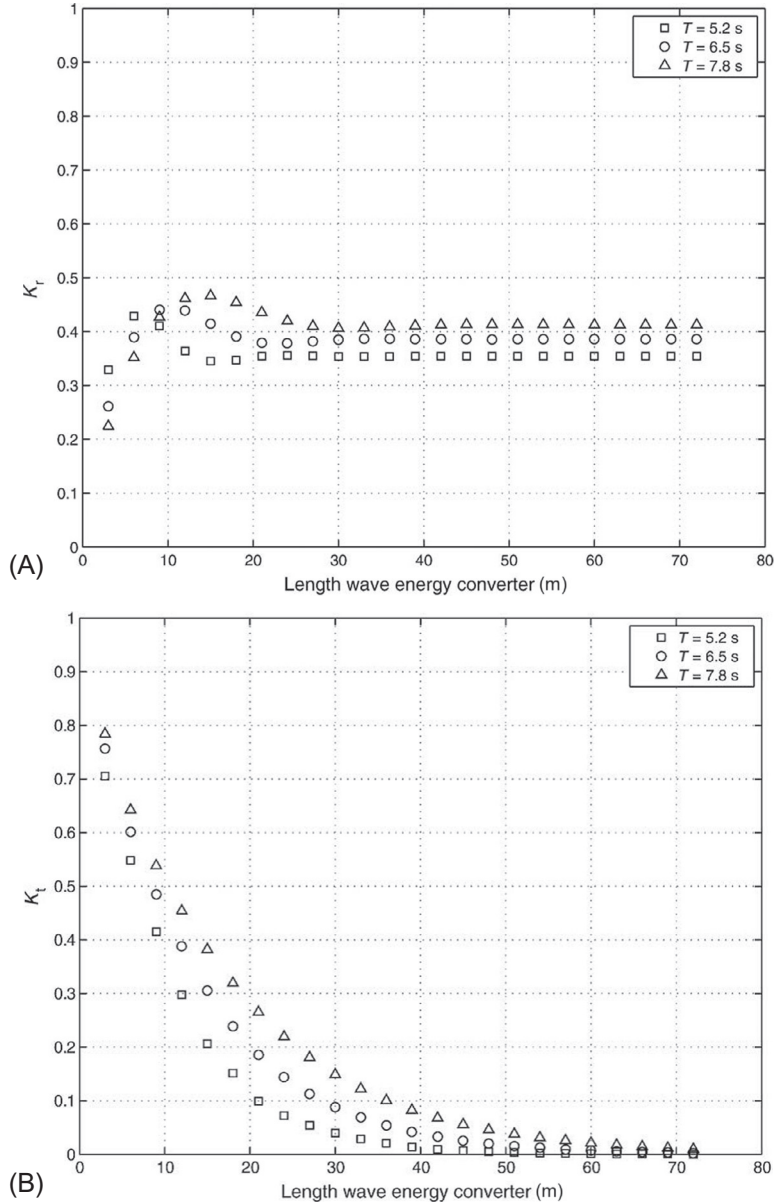


FIG. 10.6 (A) Reflection coefficient K_r , and (B) transmission coefficient K_t , for WECs with a constant absorption coefficient $S=0.9$ and increasing length for regular waves with wave periods of respectively 5.2, 6.5, and 7.8 s.

coefficients and absorption function need to be tuned for each sea-state to not only match the WEC power absorption characteristic, but also its intrinsic frequency dependence.

As an example, consider a WEC of 36 m and incident irregular long-crested waves with $H_s=1 \text{ m}$, $T_p=5.2 \text{ s}$ and $\gamma=3.3$. The corresponding overall absorption equals 37% (=the total

absorbed wave power in kW/m for all frequencies divided by the wave power in the incident wave) and K_r is assumed to be smaller than 0.1 so that the amount of reflected wave power can be neglected. The resulting transmitted wave spectrum is shown in Fig. 10.7B, where a comparison is made between the transmitted wave spectrum behind the WEC with an overall absorption of 37% with a frequency dependent absorption as specified by the developer on the one hand and an intrinsic frequency dependent absorption as discussed previously.

In both cases the transmitted significant wave height is 0.77 m as the overall absorption is equal, but the transmitted wave spectra differ. To correct for this the wake behind the WEC should be studied so that absorption function can be tuned to provide the correct absorbed power for each frequency component (Fig. 10.7A). This also applies to wave direction for directionally dependent WECs. The absorption function should then not only be tuned for each frequency component but also for each wave direction.

10.2.4 Implementation of the Numerical Coupling Methodology

10.2.4.1 Introduction

As mentioned in Section 10.1, both ‘wave–WEC’ models (or wave–structure interaction solver) and wave propagation models cannot be used individually to model both the park and far-field effects. However, a generic coupling methodology between the approach used for investigating park effects and the approach used for predicting far-field effects is presented, applicable for both type (a) and type (b) WECs.

This coupling methodology has been developed to combine:

1. the advantages of the approach of wave–structure interaction solvers, which accurately formulate and efficiently resolve the physical processes in wave energy absorption;

2. and the benefits of the approach of wave propagation models, which efficiently resolve the propagation and transformation of waves over large distances, including bathymetric variability over the WEC farm area and wave transformation processes when approaching a coastline.

Moreover, the application of a new wave generation technique is presented to generate the perturbed or radiated wave field induced by an (oscillating) WEC in a wave propagation model. This coupling methodology was initially presented by Troch and Beels (2009) and extended significantly by Stratigaki (2014).

10.2.4.2 The Generic Coupling Methodology for a Single WEC or for a WEC Farm Modelled as a Whole

The generic coupling methodology, as illustrated in Fig. 10.8, consists of three steps:

- Step 1.** The wave propagation model is used to obtain the incident wave field at the location of the WECs.
- Step 2.** The obtained incident wave field from Step 1 is used as input in the wave–structure interaction solver to obtain an accurate solution of the perturbed wave field around the structure.
- Step 3.** The perturbed wave field information from Step 2 is used as input in the wave propagation model. The perturbed wave field is imposed as prescribed internal boundary wave conditions on a wave generation circle which surrounds the structure, as shown in Fig. 10.9. Using the wave propagation model, the far-field perturbed wave field (including the diffracted, and if applicable, the radiated wave fields, eg, for a type (b) WEC) is calculated.

In this way, the resulting far-field effects of a WEC (farm) can be further determined using

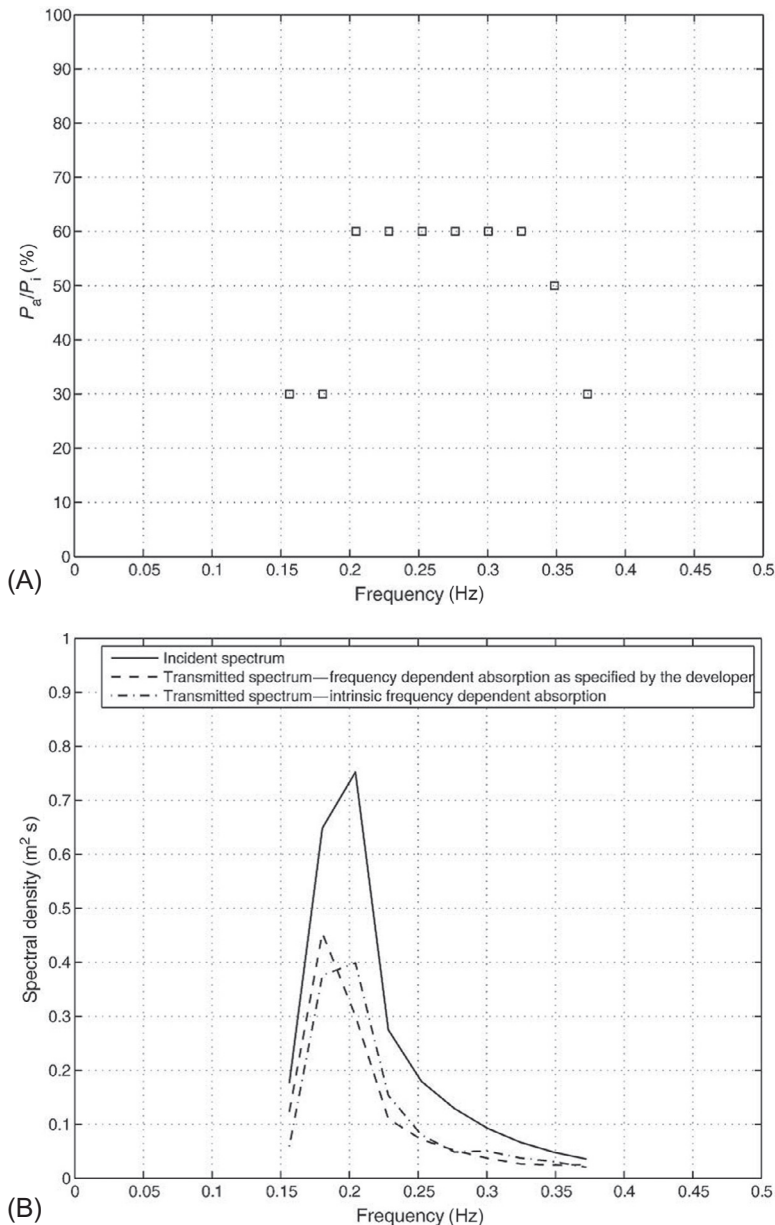


FIG. 10.7 (A) Dimensionless absorbed wave power of a WEC for 10 wave frequencies as specified by the developer. (B) Comparison of transmitted frequency spectrum for a WEC with a frequency dependent capture width ratio and with an overall capture width ratio.

the wave propagation model, in a time efficient and accurate way, taking into account both the geometric/bathymetric characteristics and wave transformation at the installation site, as well as the detailed perturbed wave field around the WEC (farm).

Fig. 10.9 represents the numerical domain in the wave propagation model when the coupling

methodology is used. The WEC or WEC farm (modelled as a single entity) is implemented using the wave generation circle upon which prescribed internal boundary wave conditions are imposed, for the perturbed wave field. In the area within the wave generation circle, a wave absorbing sponge layer is used to dissipate waves that would affect the generated wave field negatively.

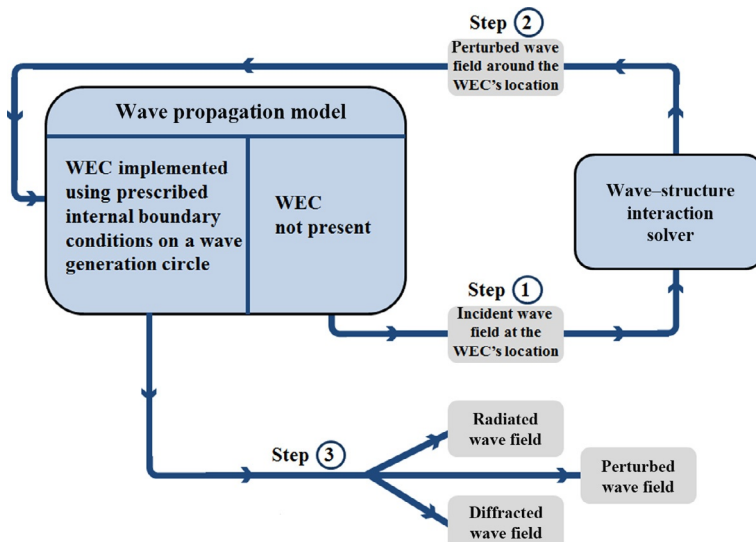


FIG. 10.8 Flow chart illustrating the step-by-step procedure for coupling a wave–structure interaction solver and a wave propagation model.

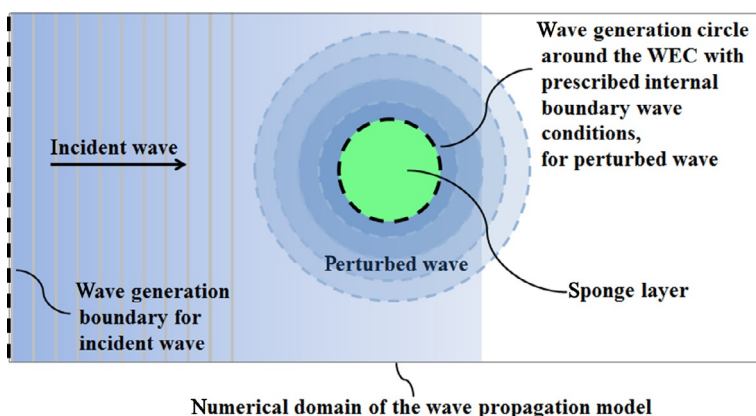


FIG. 10.9 Definition sketch of the wave generation on a circle around the WEC (or WEC farm) using prescribed internal boundary wave conditions for the perturbed wave field around the WEC (farm).

An important feature of the presented coupling methodology is that it is generic:

- any wave–structure solver or analytical expression describing the perturbed wave field [eg, the so-called Kochin function (Babarit et al., 2013)] can be used to provide the perturbed wave field used as prescribed internal boundary wave conditions.
- any wave propagation model can be used; the wave generation circle can be implemented in the numerical domain of any wave model.
- any fixed or oscillating/floating structure can be modelled.

10.2.4.3 The Generic Coupling Methodology for a WEC Farm of Individually Modelled WECs of Type (b)

To study a WEC farm composed of individually modelled single WECs, the diffracted wave field (all WECs are considered to be stationary) and the radiated wave field for each WEC (one WEC is oscillating, the other WEC(s) are stationary) are calculated separately during each time step. Consequently, if N is the number of the WECs of the farm, at each time step $N+1$ wave fields are calculated and summed (N radiated wave fields from each WEC and one diffracted wave field from the entire WEC farm).

The radiated wave field generated by each oscillating WEC is determined in two steps. Although the methodology is illustrated for a farm (or ‘system’) of two oscillating WECs, as shown in Fig. 10.10, it is generally applicable for an arbitrary number of WECs. In the first step, the diffracted wave field around each WEC caused by the incident wave in MILD-wave, η_i , is calculated separately, in order to determine the wave amplitude incident on each WEC. Furthermore, the amplitude of the radiated wave, a_w , as determined for an individual WEC of type (b) using a wave–WEC interaction solver, is multiplied by the calculated wave amplitude (from the previous step) incident on each WEC. This results in the primary radiated wave caused by the diffracted wave, η_{rad_diff} . As the wave incident on WEC 1 is not diffracted yet, the primary radiated wave of WEC 1, η_{rad_i} , is caused by the incident wave, η_i .

In the second step, the amplitude of the radiated wave of each WEC (in Fig. 10.10, WEC 1), η_{rad_diff} or η_{rad_i} , on the location of the other WEC (in Fig. 10.10, WEC 2) is calculated.

For WEC 2, this radiated wave is another incident wave which causes secondary radiated waves; ($\eta_{rad_rad_i}$ or $\eta_{rad_rad_diff}$ with $\eta_{rad_rad_i}$ the radiated wave in WEC 2 caused by the primary radiated wave η_{rad_i} of WEC 1, and with

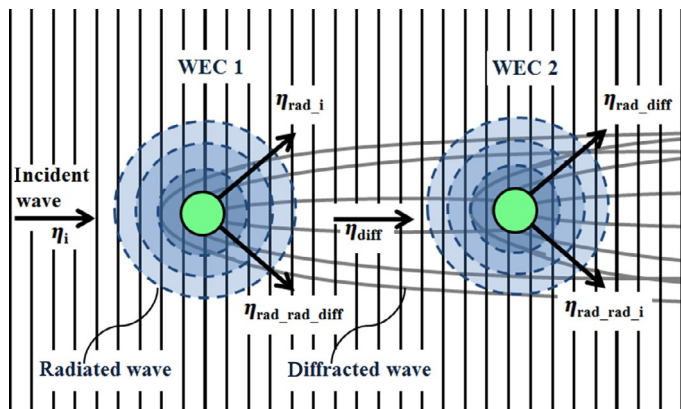


FIG. 10.10 Definition sketch of wave field interaction between two type (b) WECs.

$\eta_{\text{rad_rad_diff}}$, the radiated wave in WEC 1, caused by the primary radiated wave of WEC 2, $\eta_{\text{rad_diff}}$).

The amplitude of $\eta_{\text{rad_rad_i}}$ is calculated by multiplying the amplitude of the radiated wave, a_w , of an individual WEC as calculated using a wave–WEC interaction solver (see previous section), by the amplitude of $\eta_{\text{rad_i}}$ in front of WEC 2. The amplitude of $\eta_{\text{rad_rad_diff}}$ is calculated by multiplying the amplitude of the radiated wave, a_w , of an individual WEC as calculated using a wave–WEC interaction solver, by the amplitude of $\eta_{\text{rad_diff}}$ downwave of WEC 1.

These radiated waves could then be considered as additional incident waves on the other WEC. However, as in most cases the amplitude of these secondary radiated waves incident on the other WEC is very small compared to that of the incident wave, these secondary radiated waves are generally neglected in an ‘engineering’ approach. Therefore, only one radiated wave, determined by the diffracted/incident wave amplitude, is generated for each WEC when using the coupling methodology. A more detailed description is provided by [Stratigaki \(2014\)](#).

10.3 APPLICATIONS OF THE NUMERICAL TECHNIQUES USING MILDWAVE

10.3.1 Wake Effects by a Single WEC of Type (a)

The energy absorbing effect of a WEC reduces the wave height at its leeside. The amount of the reduction depends on the amount of absorption (absorption coefficient), the geometry (length and width) of the WEC and the incident wave climate. As an example application of the methodology presented, in [Section 10.2.3](#), the wake behind a generic type (a) WEC is studied in this section for the four irregular long-crested and short-crested sea-states provided in [Table 10.1](#).

The generic WEC is of the fixed overtopping type and has for simplicity a square plan view shape ($36 \text{ m} \times 36 \text{ m}$). The WEC has a

TABLE 10.1 Sea-States

Test	H_s (m)	T_p (s)	s_{\max}
F	1.0	5.2	—
G	1.0	7.8	—
H	1.0	5.2	75
I	1.0	5.2	100

prespecified capture width ratio of 45% and a prespecified overall reflection coefficient of 0.14. The capture width ratio is defined as the ratio between the absorbed power and the wave power incident on a wave-front width equal to the width of the WEC.

The amounts of reflection and absorption of the generic WEC are tuned in a numerical wave flume with a width of 36 m. The edge cells of the WEC have been assigned an absorption coefficient with a value of 0.975 to obtain the correct amount of reflection ([Fig. 10.4](#)) while the absorption coefficient increases to 1.0 through the WEC to produce the required transmission coefficient and consequently to obtain a capture width ratio of 45%. Without the technique of decoupling the reflection and transmission, only an absorption of 90% would have been possible with an overall reflection coefficient of 0.14, as seen in [Fig. 10.5](#).

The values of the absorption coefficient through the WEC are tuned separately for each peak wave period, since the absorption is frequency dependent. Depending on the type of WEC, the capture width ratio could vary with mean incident wave direction; however only head-on waves are considered in this study.

The disturbance coefficients K_d , the ratio of the disturbed to incident significant wave height, in a wave basin with a single WEC for long-crested waves (head-on) with peak wave periods of respectively 5.2 and 7.8 s (test cases F and G) are shown in [Fig. 10.11A and B](#) (the position of the WEC is indicated by a white square).

A small wave height increase at the edges of the wake due to diffraction is observed for both

wave periods. The wave height decrease behind the WEC is smaller for a peak wave period of 7.8 s, approximately 0.175 m, compared to 0.225 m for a peak period of 5.2 s. Furthermore, the wave shadow is wider for the longer wave period. This result indicates that the peak wave length will influence the optimal pattern of a

farm where a WEC should avoid the centre of the wake location of a neighbouring WEC.

The disturbance coefficients around a single WEC for short-crested waves, where the directional width is increasing from ~9 degrees ($s_{\max}=75$) up to 24 degrees ($s_{\max}=10$) for the peak period, are shown in Fig. 10.11C and D,

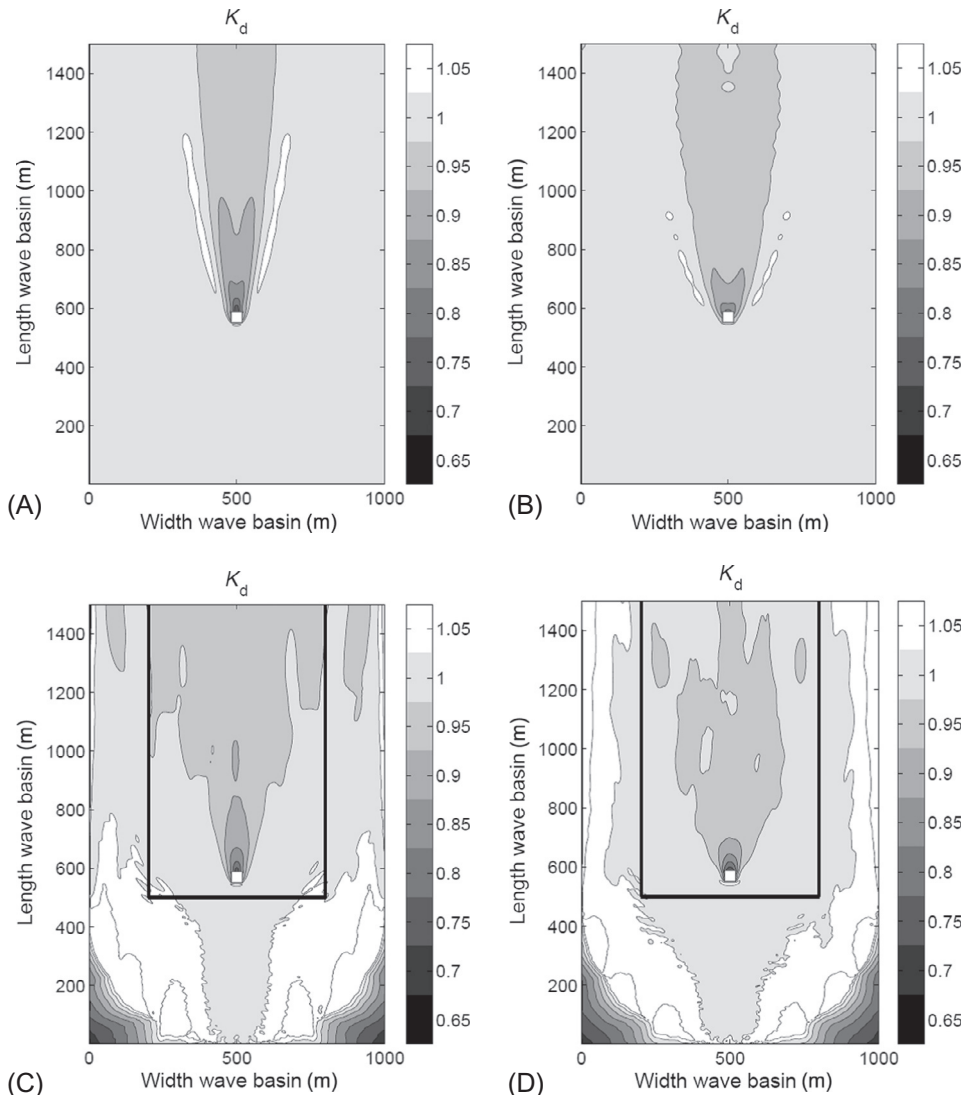


FIG. 10.11 Disturbance coefficient K_d in a wave basin with an individual WEC (capture width ratio = 45%) for irregular long-crested waves (head-on) with respectively $T_p=5.2$ s (A), $T_p=7.8$ s (B) and for irregular short-crested waves (head-on—useful domain indicated with black lines) with $T_p=5.2$ s and respectively $s_{\max}=75$ (C), $s_{\max}=10$ (D).

where the useful domain is indicated with black lines on Fig. 10.11C and D (Beels et al., 2010a).

It is clear from Fig. 10.11 that redistribution behind a device depends on the peak period and directional spread of the incident wave climate. The higher the peak period and the greater the directional spread, the faster waves are redistributed behind the WEC.

In another application of the sponge larger technique, a real-world case of the Wave Dragon WEC has been used to study the wake effect, both for a single WEC and a farm of Wave Dragons (Beels et al., 2010b). After tuning the reflection, absorption, and transmission characteristics of the main body and the reflection to the prototype values, a study of wake effects for a single device was carried out. Fig. 10.12 shows a comparison of wake dimensions for irregular long-crested and short-crested waves with $H_s = 1$ m and $T_p = 5.6$ s. As expected, the wake shortens with increasing directional spreading due to a faster redistribution behind the WEC. A wider wake is observed for short-crested waves. More details are discussed in Beels et al., 2010b.

10.3.2 Wake Effects by a Farm of Type (a) WECs

The understanding of the impact of one WEC on the wave climate is crucial in determining the capture width ratio of the neighbouring devices in a farm. Since a single WEC reduces the wave height in its lee, the capture width ratio of a WEC installed in its lee will decrease. The reduction is determined by the dimensions and capture width ratios of the surrounding WECs, by the incident wave climate and by the separation of the WECs in the farm. The dimensions of a WEC define the diffracted wave pattern around the WEC, while the magnitude of wave height reduction in the diffracted wave pattern is depending on its capture width ratio (absorption coefficient). The incident wave climate determines the redistribution of wave energy behind the WEC, as seen in Section 10.3.1.

In this section a farm with a distance between the WECs and a separation distance of the rows of two times the WEC dimensions is implemented in MILDwave. Two different layouts with nine

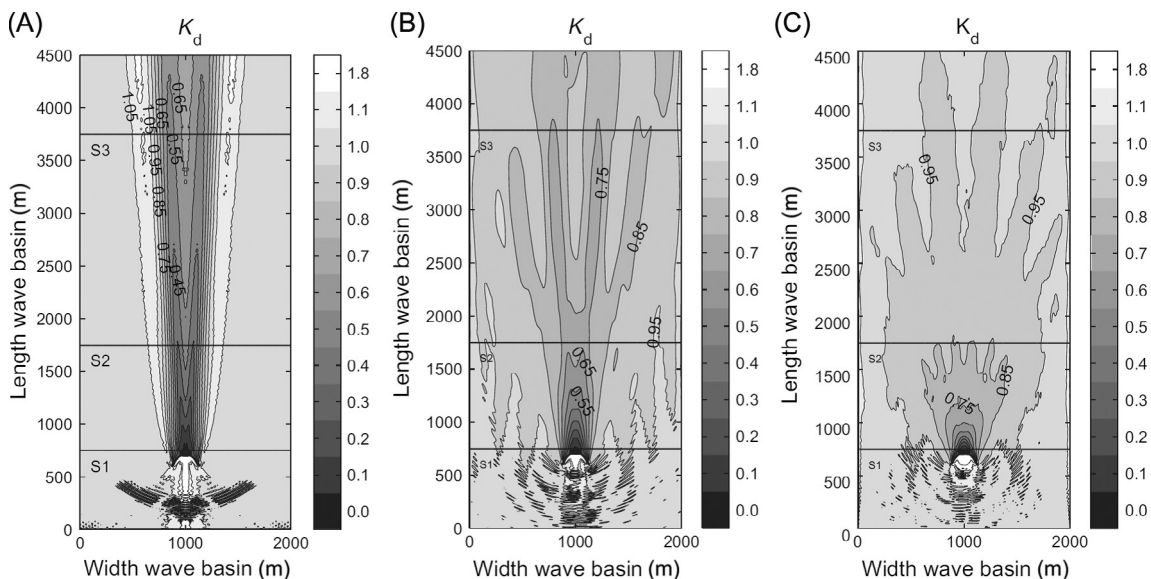


FIG. 10.12 Calculated disturbance coefficient K_d in a wave basin with a single Wave Dragon WEC for irregular (A) long-crested waves (head-on) with $T_p = 5.6$ s and short-crested waves (head-on) with $T_p = 5.6$ s and s_{\max} of respectively (B) 75 and (C) 10.

generic WECs, as defined in the previous section, are compared: a layout with three identical rows (an aligned grid), where the WECs are placed right behind each other, and a layout where the first and third row are identical, but where the second row is shifted over a distance equal to the dimension of the WEC (a staggered grid).

The capture width ratio for significant wave heights between 0.45 m (10%) and 1 m (45%) has been investigated. Each capture width ratio as a function of significant wave height H_s has been tuned in a numerical wave flume as explained in [Section 10.2.3](#). No variation with wave period is considered as only irregular long-crested waves with $H_s = 1$ m and $T_p = 5.2$ s are generated in this section. The capture width ratio decreases with decreasing wave height as observed in the power matrix of the Wave Dragon ([Sørensen et al., 2006](#)).

Due to the technique of decoupling reflection and transmission, it is possible to keep the reflection small for each defined capture width ratio and tune the amount of transmission and

consequently the absorption. The decoupling is needed to implement adaptive absorption (adapting the capture width ratio of each WEC in the farm to its incident wave height without changing the amount of reflection) to simulate a farm.

In a first step, only WECs in the first row, with the same capture width ratio as an isolated WEC (45%), are modelled. By measuring the average wave height on the positions of the WECs that will be installed in the second row and by using the capture width ratio as a function of significant wave height H_s , the capture width ratio of those WECs is derived. In a second step, WECs in the two first rows, with their calculated capture width ratios, are modelled and the wave height is measured on the positions of the WECs in the third row. The average wave height at these WEC positions is then used to define their capture width ratio.

The dimensionless calculated disturbed significant wave heights H_{sd} for both layouts are given in [Fig. 10.13A](#) and [B](#) respectively for test

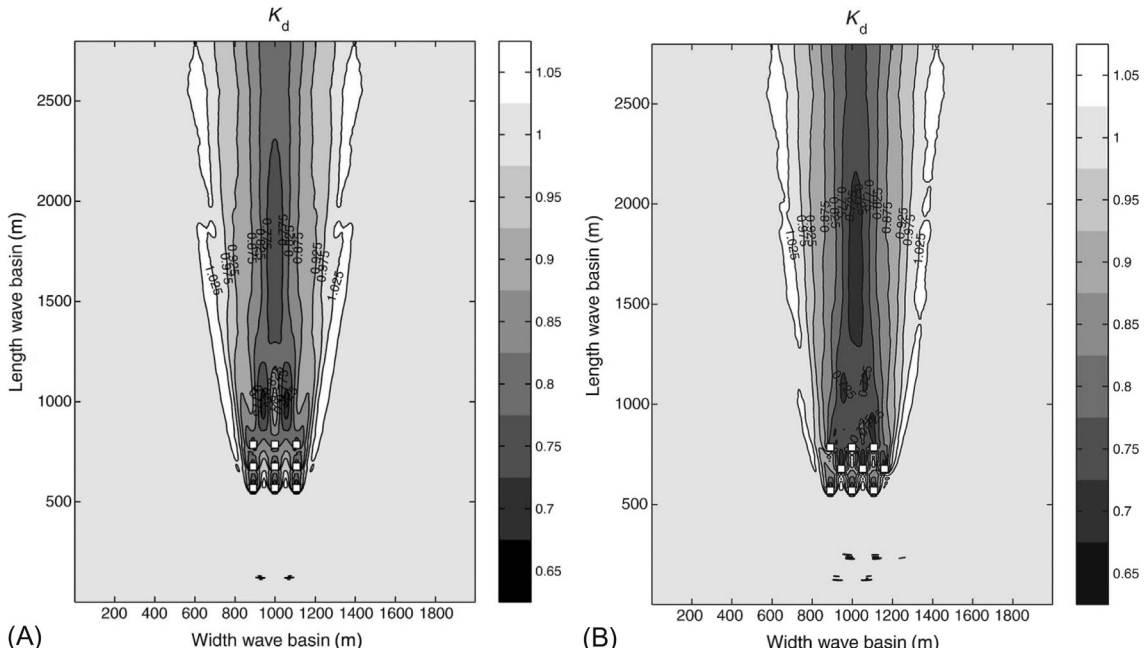


FIG. 10.13 Calculated disturbance coefficient K_d in a wave basin with nine generic WECs for irregular long-crested waves (head-on) with $T_p = 5.2$ s (test case F—(A) aligned grid, (B) staggered grid).

case F of [Table 10.1](#). It can be seen that the wave height in front of the second and third row is much higher for the staggered grid, which results in a higher capture width ratio for the WECs in those rows (capture width ratio of respectively

45% and 35% for the second and third row) compared to the aligned grid (capture width ratio of 30% for the second and third row).

[Fig. 10.14A and B](#) shows a transverse section right behind the farm and a longitudinal section

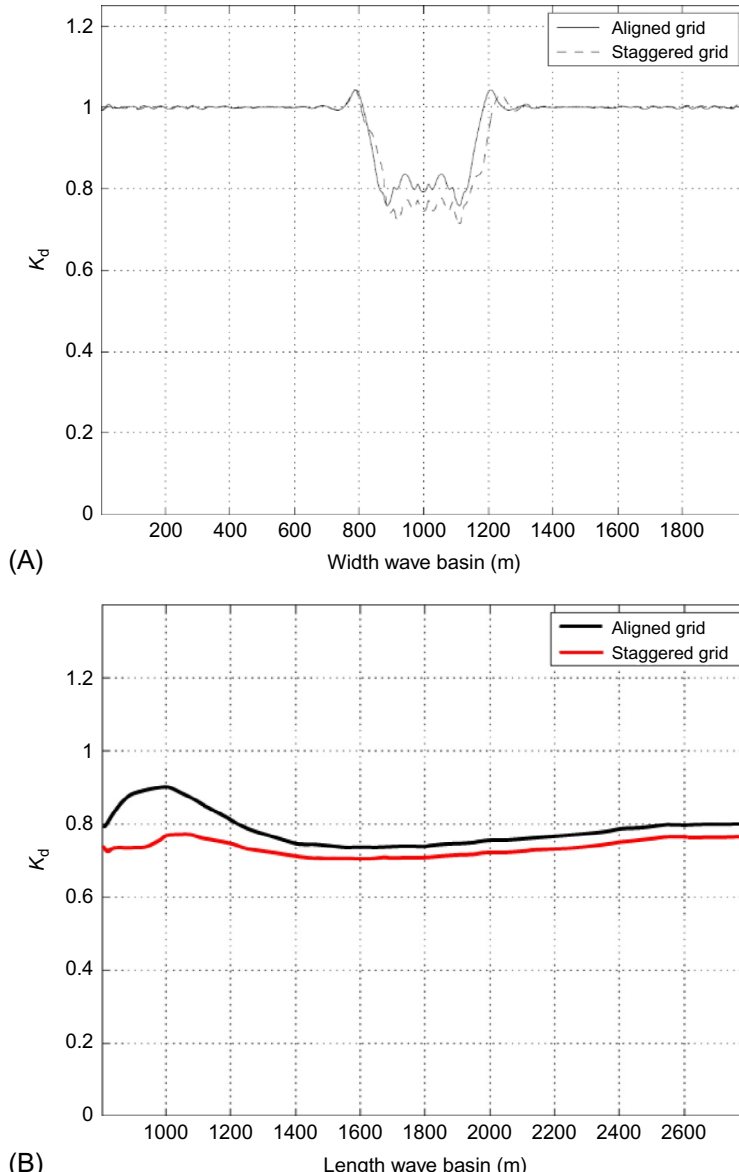


FIG. 10.14 Disturbance coefficient K_d for an aligned and a staggered layout from [Figs 10.13A](#) and [10.13B](#), (A) in a lateral cross section at $y = 805$ m; (B) in a longitudinal cross section at $x = 1000$ m behind the WECs.

behind the farm for both layouts. The wave height is lower (higher wave height reduction) behind the staggered grid compared to the aligned grid due to the higher capture width ratio of the WECs in the second and third row. If a constant capture width ratio (no adaptive absorption) was used for all WECs in the farm, the difference between both layouts would be very small. With this methodology, the power absorbed by a farm and the coastal impact of a farm can be studied relatively quickly.

10.3.3 Wake Effects by a Single Type (b) WEC

10.3.3.1 The Modelled WEC

As an example of the implementation and validation of the presented generic coupling methodology described in [Section 10.2.4.2](#), a heaving WEC with one degree of freedom (DOF) is modelled ([Stratigaki, 2014](#); [Stratigaki et al., 2016](#)). A detailed description of the WEC geometry, response and power take-off system is provided by [Stratigaki et al. \(2014, 2015\)](#). Summarized, the WEC consists of a buoy, with hemispherical bottom and a cylindrical vertical body (total height of 60.0 cm). The buoy's draught is 31.5 cm, equal to its diameter, D , with a total mass, $m = 20.490$ kg.

The hydrodynamic interaction between the modelled heaving WEC and the incident wave field is modelled using the hydrodynamic solver ([WAMIT, 2016](#)). No damping is applied on the WEC through the power take-off (PTO) system and therefore the results presented here refer to an undamped WEC. Far-field effects have been modelled using the coupling methodology implemented in MILDwave.

10.3.3.2 Wave Conditions and Numerical Domains

The wave diffraction and radiation wave fields of the WEC are investigated for a regular wave with direction $\theta = 90$ degrees and amplitude $a = 0.037$ m, period $T = 1.26$ s, constant water depth $d_w = 0.70$ m and wavelength $L = 2.384$ m ([Stratigaki et al., 2014, 2015](#)).

In MILDwave, a computational domain with wave absorbing sponge layers is implemented to provide an effective domain (area without the sponge layers) of 49.7 m \times 39.2 m ($w_d \times l_d$), which has been discretized using grid cell size, $\Delta x = \Delta y = 0.018$ m. In WAMIT, a much smaller area of 10.0 m \times 10.0 m around the WEC is modelled, using grid cell size, $\Delta x = \Delta y = 0.100$ m for the free-surface elevation output points. In the middle of the grid cells, the wave amplitude, a , and phase shift, φ , are calculated.

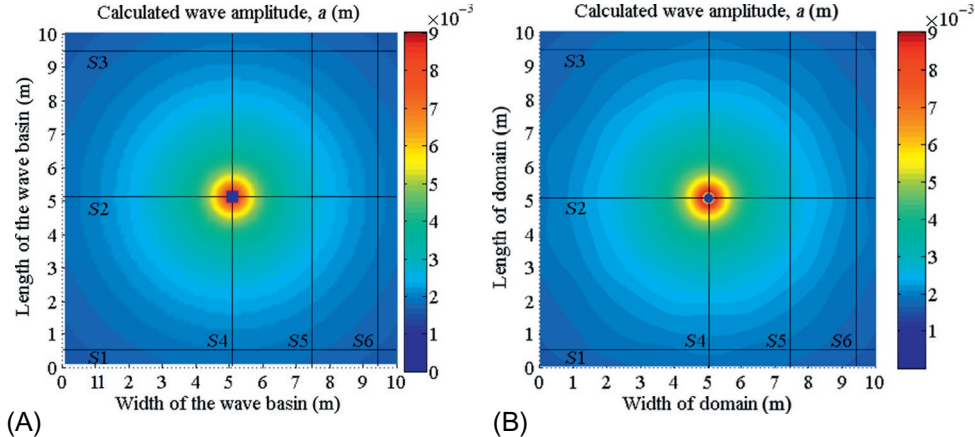
In order to compare the obtained MILDwave results to WAMIT results, the same area around the WEC is considered in both models (10.0 m \times 10.0 m). For the perturbed wave field, the two models are compared for a domain with extended dimensions, 49.6 m \times 39.2 m ($w_d \times l_d$).

10.3.3.3 Modelling and Verification of the Radiated, Diffracted, and Perturbed Wave Fields Using the Coupling Methodology

The radiated, diffracted, and perturbed wave fields are simulated and compared for both models.

For the *radiated wave field*, the wave amplitude, a , and phase shift, φ , relative to the centre of the WEC, are shown in [Fig. 10.15\(i\)](#) and [\(ii\)](#), respectively, for the radiation problem as calculated using (A) WAMIT and (B) MILDwave. In WAMIT, the WEC is implemented as a heaving structure, placed in the centre of the numerical domain. In MILDwave, the WEC is implemented as a wave source realized by a wave generation circle with a radius ($r_C = 0.20$ m) slightly larger than the WEC radius (0.1575 m). Waves are generated only on a wave generation circle using the technique described in [Section 10.2.2](#). The results in the circular area with radius $r < r_C$ (where $r_C = 0.20$ m) and (x_C, y_C) in the centre of the domain in MILDwave, are set to zero; the values within the wave generation circle have no physical meaning, as this area corresponds to a wave absorbing sponge layer inside the wave generation circle.

(i) Wave amplitude



(ii) Phase shift

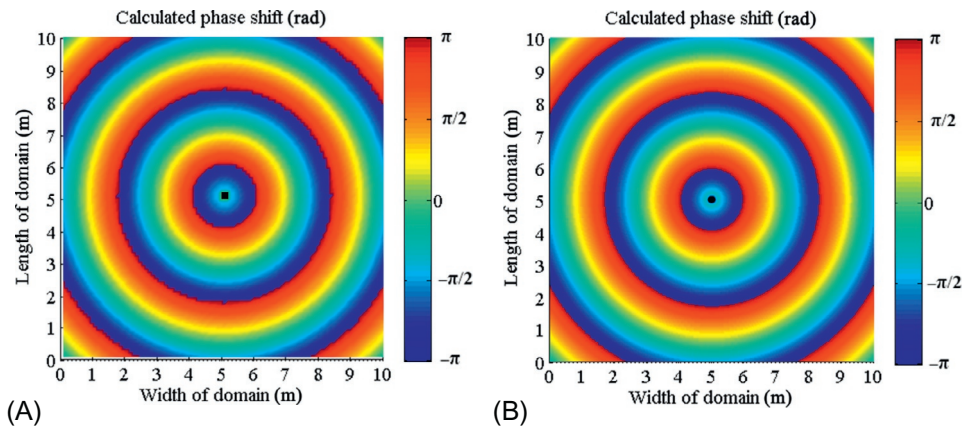


FIG. 10.15 Calculated (i) wave amplitude, a , and (ii) phase shift, φ , for the radiated wave field around a heaving WEC in (A) WAMIT and in (B) MILDwave. The radiated waves propagate in all directions from the source. The propagating incident waves are not shown in (i).

In Fig. 10.16A and B, the calculated wave amplitude, a , for the radiated wave field in WAMIT and MILDwave are compared in sections (S1) and (S4) as indicated on Fig. 10.15A and B, respectively. Very good agreement is observed between the WAMIT and MILDwave results. Very small deviations are seen only on the wave generation circle, in the section through the WEC (S4). However, the results on the wave generation circle are not taken

into account for this comparison. Detailed verification results for the diffracted and the perturbed wave fields are presented in Stratigaki et al. (2016) and Stratigaki (2014).

The diffracted wave field is modelled and compared for the two models. For simplicity, the WEC is modelled as a fully reflecting fixed structure in MILDwave. However, by using the sponge layer technique described in Section 10.2.3, different amounts of wave energy

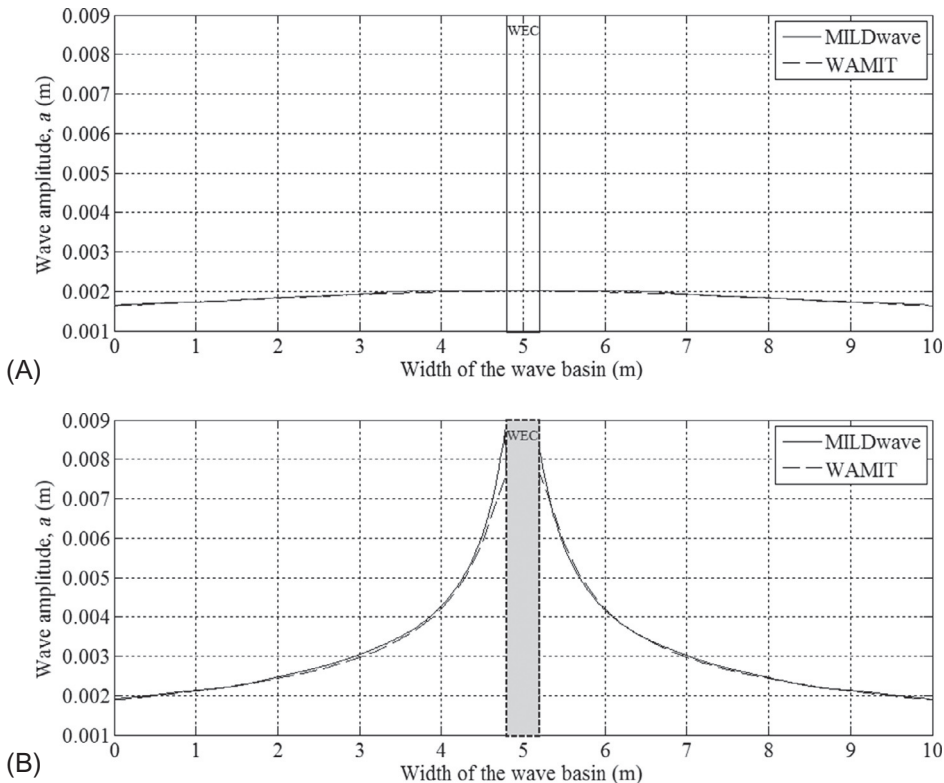


FIG. 10.16 Calculated wave amplitude, a , in sections (A) section S1 = section S3 = section S6 and (B) section S4 = section S2, in WAMIT and MILDwave.

absorption by the WEC could be modelled. Diffraction is modelled intrinsically in MILDwave, while waves are generated along a wave generation line. As both MILDwave and WAMIT are based on potential-flow theory, the resulting diffracted wave fields compare very well to each other.

Finally, the resulting *perturbed wave field* around the heaving WEC under incident waves is modelled. In MILDwave, at each time step, the diffracted and radiated wave fields are calculated separately and afterwards the wave elevations and velocity potentials are summed up. By separating the calculation of both wave fields, the diffracted wave is not disturbed by the wave absorbing sponge inside the wave generation circle. On the other hand, the radiated wave is not disturbed by the fully reflecting structure

(or structure with specific absorption coefficients assigned, in another case) used for the simulation of the diffracted wave field. The WEC is implemented as an oscillating fully reflecting structure surrounded by the wave generation circle, and is placed in the centre of the numerical domain. The waves are simultaneously generated along a wave generation line and on a wave generation circle, using the coupling methodology. For the calculation of the perturbed wave field in MILDwave, an additional phase shift, φ , between the radiated and diffracted wave field is necessary, which is obtained using the WAMIT results as presented by Stratigaki (2014) and Stratigaki et al. (2016). The calculated wave amplitudes, a , for the perturbed wave field in WAMIT and in MILDwave (with the coupling methodology implemented)

are compared in the extended sections ($S1$) and ($S4$) indicated in Fig. 10.15(i). By pursuing an 'engineering' approach, the near-field area around the WEC is not considered. Based on practical considerations, this area is taken equal to a circle with radius $5D$, considered to be the shortest practical WEC separation distance in a WEC farm. Outside of this area, MILDwave results are compared to WAMIT results to evaluate the achieved accuracy of the presented coupling methodology. A very good agreement is observed in the far field (Stratigaki, 2014; Stratigaki et al., 2016). The differences between the wave amplitudes, a , for the perturbed wave field calculated using WAMIT and MILDwave (with the coupling methodology implemented) do not exceed in the extended section $S1$ 3.3%, while the largest difference at the far field (at a large distance from the WEC) reduces to 1.8%.

The absolute difference in wave amplitude, a , between WAMIT and MILDwave is calculated as:

$$\left| \frac{a_M - a_W}{a_W} \right| \times 100\% \quad (10.2)$$

where a_M , the calculated wave amplitude in MILDwave and a_W , the calculated wave amplitude in WAMIT.

The differences calculated using (Eq. 10.2), are shown in Fig. 10.17A and B, for the $10.0\text{ m} \times 10.0\text{ m}$ and the $49.6\text{ m} \times 39.2\text{ m}$ numerical domains, respectively.

In order to visualize the effect of these differences for the studied case, two circles have been drawn in Fig. 10.17A. The radius of the inner circle is equal to $5D$, and within this area, the results are not used for performance comparison between the two models. As a result, when a WEC is added at a distance of $5D$ in front of and/or in the lee of the WEC shown in Fig. 10.17A, the largest wave amplitude differences that the new WEC(s) will experience, when the coupling methodology implemented in MILDwave is used, do not exceed 8.0%. Most importantly, this wave amplitude difference of 8.0% represents two local peaks in front of and in the lee of the WEC, as shown in detail by Stratigaki (2014) and Stratigaki et al. (2016). Moreover, as presented in Fig. 10.17, the largest wave amplitude differences (16.5%) appear in the lee of the WEC

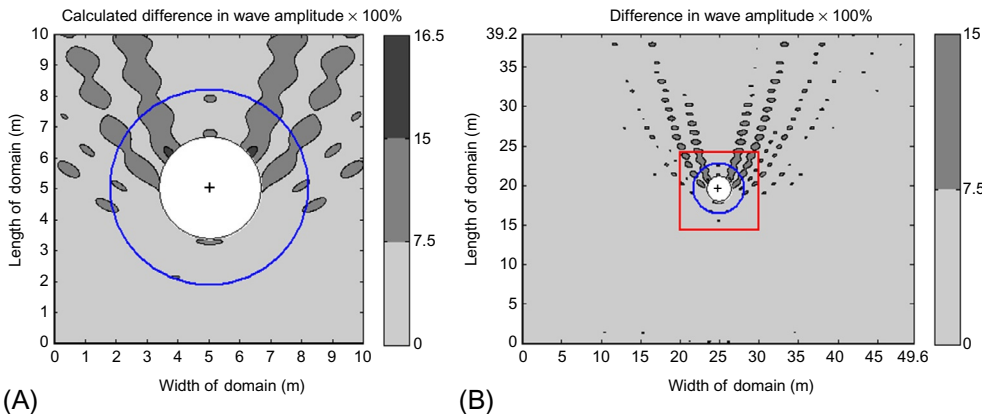


FIG. 10.17 Calculated (using Eq. 10.2) wave amplitude differences between WAMIT and MILDwave (with the coupling methodology implemented), for the perturbed wave field around a heaving WEC: a domain is shown with dimensions (A) $10.0\text{ m} \times 10.0\text{ m}$ ($w_d \times l_d$), and (B) $49.6\text{ m} \times 39.2\text{ m}$. Light grey, grey, and dark grey colour represent areas with differences smaller than 7.5%, between 7.5% and 15.0%, and max 16.5%, respectively. The zones within the drawn inner and outer circles are indicated, with diameters $5D$ and $10D$, respectively, where D is the WEC diameter. The '+'-symbol indicates the WEC centre. The drawn square indicates the limits of the $10.0\text{ m} \times 10.0\text{ m}$ domain shown in (A).

at ± 45 degrees, and are spatially very limited and localized effects.

Therefore, the coupling methodology implemented in the wave propagation model MILDwave is suitable for modelling far-field effects of the modelled WEC. In the largest part of the $49.6 \text{ m} \times 39.2 \text{ m}$ domain, and especially in front and in the lee of the WEC and in the far field, the wave amplitude differences are very small, which confirms the good agreement between the results obtained using WAMIT and MILDwave (with the coupling methodology implemented).

10.4 LIMITATIONS

The use of phase-resolving wave propagation models based on the mild-slope equations will have limitations inherited from the propagation model itself. Thus, there is a limitation to the seabed slope, which must typically be less than $1/3$. In addition, because the wave propagation model is based on a linear model the accuracy of the model reduces in shallow water and for very steep waves due to their inherent nonlinearity. However, this limitation can be reduced, at least for shallow water, with the use of a Boussinesq model, although this then introduces other potential limitations associated with the model numerical stability.

A limitation also exists in that the implementation of reflection, transmission, and absorption characteristics of a WEC requires empirically fine-tuning of the absorption function (using data from another model such as a BEM model—see Chapter 3—or wave-tank model data) to achieve the required reflection, transmission, and absorption characteristics. Thus, the accuracy of WEC array interactions and far-field effects calculated using a phase-resolving wave propagation model is dependent on the accuracy of the underlying model data used to define the sponge layer characteristics. Similarly, the surface elevations and phase

angles defined on the generation circle to represent the radiated waves must also be generated externally. Again, the limitations in accuracy of the external model will be reflected in the accuracy of the WEC array interactions and far-field effects.

Finally, current implementations of phase-resolving models do not include the modelling of the WEC response that is required to define the amplitude of the radiated waves. There is no fundamental reason why this could not be included in a bespoke phase-resolving model; however, the lack of implementation of this type of model means that this is currently a limitation.

10.5 SUMMARY

- Phase-resolving wave propagation models used to model WEC arrays may be based on the time-dependent mild-slope equations, for example MILDwave.
- WECs may be represented in the model as type (a), with no wave radiation, or type (b), where wave radiation is included.
- A tuned sponge layer, with the same size as the WEC, can be used to obtain the required amount of reflected, transmitted, and absorbed wave energy.
- Radiated waves can be modelled using a circular wave generation line surrounding the WEC.
- The required reflected, transmitted, absorption, and radiation characteristics must be defined externally, for example using a potential-flow model or wave-tank/field data.
- A minimum length of sponge layer is required to achieve higher levels of wave absorption.
- The wave fields generated using a tuned phase-resolving wave propagation model agree well with those produced using a potential-flow model such as WAMIT.

- The numerical coupling methodology presented in this chapter combines the advantages of wave–structure interaction solvers with the benefits of wave propagation models, yielding a cost-effective and accurate tool/methodology.

References

- Babarit, A., Folley, M., Charrayre, F., Peyrard, C., Benoit, M., 2013. On the modeling of WECs in wave models using far field coefficients. In: Proceedings EWTEC2013, Aalborg, Denmark.
- Beels, C., Troch, P., De Backer, G., Vantorre, M., De Rouck, J., 2010a. Numerical implementation and sensitivity analysis of a wave energy converter in a time-dependent mild-slope equation model. *Coast. Eng.* 57 (5), 471–492.
- Beels, C., Troch, P., De Visch, K., Kofoed, J.P., De Backer, G., 2010b. Application of the time-dependent mild-slope equations for the simulation of wake effects in the lee of a farm of Wave Dragon wave energy converters. *Renew. Energy* 35, 1644–1661.
- Beels, C., Troch, P., Kofoed, J.P., Frigaard, P., Vindahl Kringselum, J., Carsten Kromann, P., Heyman Donovan, M., De Rouck, J., De Backer, G., 2010c. A methodology for production and cost assessment of a farm of wave energy converters. *Renew. Energy* 36 (12), 3402–3416.
- Berkhoff, J.C.W., 1972. Computation of combined refraction-diffraction. In: Proceedings of 13th Conference on Coastal Engineering, Vancouver, pp. 471–490.
- Booij, N., 1983. A note on the accuracy of the mild-slope equation. *Coast. Eng.* 7, 191–203.
- Brorsen, M., Helm-Petersen, J., 1998. On the reflection of short-crested waves in numerical models. In: Proceedings of the 26th International Conference on Coastal Engineering, Copenhagen, pp. 394–407.
- Copeland, G.J.M., 1985. A practical alternative to the mild-slope wave equation. *Coast. Eng.* 9, 125–149.
- Dingemans, M.W., 1997. Water wave propagation over uneven bottoms. In: Liu, P.L.F. (Ed.), Series on Ocean Engineering, vol. 13. World Scientific, Singapore.
- Gruwez, V., Bolle, A., Verwaest, T., Hassan, W., 2012a. Numerical and physical modelling of wave penetration in Oostende harbour during severe storm conditions. In: 5th SCACR International Short Conference on Applied Coastal Research: Proceedings, Jun. 6th–9th, 2011. Mitteilungen des Lehrstuhls und Instituts für Wasserbau und Wasserwirtschaft der Rheinisch-Westfälischen Technischen Hochschule Aachen, 165. RWTH Aachen University, Aachen, pp. 198–205.
- Gruwez, V., Bolle, A., Verwaest, T., 2012b. Numerical modelling of wave penetration, comparison with physical model and field measurements in Zeebrugge harbour. In: Proceedings of the 4th International Conference on the Application of Physical Modelling to Port and Coastal Protection—Coastlab12, Sep. 17th–20th, 2012. Ghent University, Ghent.
- Kofoed, J.P., Margheritini, L., Stratigaki, V., Troch, P., 2008. Estimation of Wave Conditions for SSG Breakwater at Svāheia SSG Pilot Site. Department of Civil Engineering, Aalborg University, Aalborg. DCE Contract Reports 52, 154 pp.
- Lee, C., Suh, K.D., 1998. Internal generation of waves for time-dependent mildslope equations. *Coast. Eng.* 34, 35–57.
- Madsen, P.A., Sørensen, O.R., 1992. A new form of the Boussinesq equations with improved linear dispersion characteristics. Part 2: a slowly-varying bathymetry. *Coast. Eng.* 18, 183–204.
- Margheritini, L., Kofoed, J.P., Stratigaki, V., Troch, P., 2010. Estimation of Wave Conditions for SSG Breakwater at Hanstholm Location. Department of Civil Engineering, Aalborg University, Aalborg. DCE Contract Reports 90, 78 pp.
- Margheritini, L., Frigaard, P., Stratigaki, V., 2011. Characterization of wave climate at Hanstholm location with focus on the ratio between average and extreme waves heights. In: 9th EWTEC2011, Sep. 5–9, 2011, Southampton, UK.
- Margheritini, L., Stratigaki, V., Troch, P., 2012. Geometry optimization of an overtopping wave energy device implemented into the new breakwater of the Hanstholm Port expansion. In: Proceedings of the Twenty-Second (2012) International Offshore and Polar Engineering Conference—ISOPE 2012, Rhodes, Greece.
- McNatt, C., Venugopal, V., Forehand, D., 2013. The cylindrical wave field of wave energy converters. *Int. J. Mar. Energy* 3 (4), 26–39.
- Mei, C.C., Stiassnie, M., Yue, D.K.P., 2005. Theory and Applications of Ocean Surface Waves. Part 1, Linear Aspects. World Scientific, Singapore.
- Mendes, L., Palha, A., Conceicao, J.F., Brito-Melo, A., Sarmento, A.J.N.A., 2008. Analysis of the impact of a pilot zone for wave energy conversion offshore Portugal. In: Proceedings of the 18th International Offshore and Polar Engineering Conference (ISOPE), Vancouver, British Columbia, Canada.
- Radder, A.C., 1979. On the parabolic equation method for water-wave propagation. *J. Fluid Mech.* 95, 159–176.
- Radder, A.C., Dingemans, M.W., 1985. Canonical equations for almost periodic, weakly nonlinear gravity waves. *Wave Motion* 7, 473–485.
- Sørensen, H.C. et.al., 2006. Sea Testing and optimisation of power production on a scale 1:4.5 Test Rig of the Offshore Wave Energy Converter Wave Dragon Final Technical Report for the period October 2002 to March 2006, European Commission Contract No: ENKS-CT-2002-00603, SPOK, Copenhagen, Denmark, 82pp.

- Stratigaki, V., 2014. Experimental Study and Numerical Modelling of Intra-Array Interactions and Extra-Array Effects of Wave Energy Converter Arrays (Ph.D. dissertation). Faculty of Engineering and Architecture, Ghent University, Ghent.
- Stratigaki, V., Troch, P., 2010a. Design of Ostend Harbour: Numerical Simulation of Wave Diffraction Through the Gap at Montgomery Dock Using the 'Mild Slope' Wave Propagation Model, MILDwave. Flemish Government, Brussels. Report for Flemish Government.
- Stratigaki, V., Troch, P., 2010b. Wave Propagation Over the Thornton Bank (Belgium) Using the 'Mild Slope' Wave Propagation Model, MILDwave. Department of Civil Engineering, Ghent University, Ghent. Internal Report.
- Stratigaki, V., Troch, P., 2012a. An Introduction to the Wave Propagation Model MILDwave. Department of Civil Engineering, Ghent University, Ghent.
- Stratigaki, V., Troch, P., 2012b. MILDwave simulatie van golfvoortplanting langsheen de Vlaamse baaien m.b.v. de 'mild-slope' golfvoortplantingsmodel, MILDwave. Department of Civil Engineering, Ghent University, Ghent. (in Dutch), Internal Report.
- Stratigaki, V., Vanneste, D., Troch, P., Gysens, S., Willems, M., 2010. Numerical modeling of wave penetration in Ostend harbour. In: Proceedings of the International Conference on Coastal Engineering, No. 32 (2010), Shanghai, China. Paper #790: waves.42. <http://journals.tdl.org/ICCE/>.
- Stratigaki, V., Troch, P., Baelus, L., Keppens, Y., 2011. Introducing wave regeneration by wind in a mild-slope wave propagation model, MILDwave, to investigate the wake effects in the lee of a farm of wave energy converters. In: Proceedings of the ASME, 2011, 30th International Conference on Ocean, Offshore and Arctic Engineering (OMAE 2011), Rotterdam, The Netherlands. <http://dx.doi.org/10.1115/OMAE2011-49347>.
- Stratigaki, V., Troch, P., Malherbe, B., Forehand, J., 2012a. Vlaamse Baaien development plan: estimation of the wave climate for Flanders Bays using the numerical model MILDwave. Proceedings of the 4th International Conference on the Application of Physical Modelling to Port and Coastal Protection—Coastlab12, Sep. 17th–20th, 2012 Ghent University, Ghent.
- Stratigaki, V., Troch, P., Margheritini, L., Kofoed, J.P., 2012b. Estimation of wave conditions along a new breakwater for the Hanstholm harbour, using the numerical model MILDwave. In: Proceedings of the Twenty-second (2012) International Offshore and Polar Engineering Conference—ISOPE 2012, Rhodes, Greece.
- Stratigaki, V., Troch, P., Stallard, T., Forehand, D., Kofoed, J.P., Folley, M., Benoit, M., Babarit, A., Kirkegaard, J., 2014. Wave basin experiments with large wave energy converter arrays to study interactions between the converters and effects on other users in the sea and the coastal area. Energies 7, 701–734. <http://dx.doi.org/10.3390/en7020701>.
- Stratigaki, V., Troch, P., Forehand, D. (2016). A coupling methodology to model near and far field effects of structures and wave energy converters due to wave interaction. Accepted for publication in the proceedings of the 35th International Conference on Coastal Engineering (ICCE), Istanbul, Turkey, 17–22 July 2016.
- Stratigaki, V., Troch, P., Stallard, T., Forehand, D., Folley, M., Kofoed, J.P., Benoit, M., Babarit, A., Vantorre, M., Kirkegaard, J., 2015. Sea-state modification and heaving float interaction factors from physical modelling of arrays of wave energy converters. J. Renew. Sustain. Ener. 7, 061705. <http://dx.doi.org/10.1063/1.4938030>.
- Suh, K.D., Lee, C., Park, W.S., 1997. Time-dependent equations for wave propagation on rapidly varying topography. Coast. Eng. 32, 91–117.
- Troch, P., 1998. MILDwave—A Numerical Model for Propagation and Transformation of Linear Water Waves. Department of Civil Engineering, Ghent University, Ghent. Internal Report.
- Troch, P., Beels, C., 2009. Wave Generation on a Circle Using the Wave Propagation Model MILDwave. Department of Civil Engineering, Ghent University, Ghent.
- Troch, P., Beels, C., De Rouck, J., De Backer, G., 2010. Wake effects behind a farm of wave energy converters for irregular long-crested and short-crested waves. In: Proceedings of the International Conference on Coastal Engineering, No. 32 (2010), Shanghai, China. Paper #: waves.22, <http://journals.tdl.org/ICCE/>.
- Venugopal, V., Smith, G.H., 2007. Wave climate investigation for an array of wave power devices. In: Proceedings of the 7th European Wave and Tidal Energy Conference (2007), Porto.
- Vidal, C., Mendez, F.J., Diaz, G., Legaz, R., 2007. Impact of Santona WEC installation on the littoral processes. In: Proceedings of the 7th European Wave and Tidal Energy Conference (EWTEC), Porto, Portugal.
- WAMIT, 2016. User manual. <http://www.wamit.com/manual.htm> (accessed 15.01.16.).